

Numerical study on the feasibility of offshore single blade installation by floating crane vessels

Yuna Zhao^{a,c,*}, Zhengshun Cheng^{a,b,c}, Zhen Gao^{a,b,c}, Peter Christian Sandvik^d, Torgeir Moan^{a,b,c}

^a*Centre for Autonomous Marine Operations and Systems (AMOS),
NTNU, NO-7491 Trondheim, Norway*

^b*Centre for Ship and Ocean Structures (CeSOS), NTNU, NO-7491 Trondheim, Norway*

^c*Department of Marine Technology, NTNU, NO-7491 Trondheim, Norway*

^d*PC Sandvik Marine, Trondheim, Norway*

Abstract

Compared with jack-up crane vessels that are now widely used in offshore wind turbine installation, floating crane vessels are more flexible with respect to working water depth and are much faster in relocation. They are thus a promising alternative to install offshore wind turbine components, especially in intermediate and deep water. However, the wave-induced motions of the floating vessels make the operations challenging. This study deals with a preliminary feasibility study on offshore single blade installation using floating crane vessels. Two typical floating crane vessels are considered, i.e., a mono-hull vessel and a semi-submersible vessel. They are assumed to be equipped with dynamic positioning systems that can well mitigate the slowly varying horizontal motions. Their overall performance during the blade installation is numerically evaluated by comparing their performance against a typical jack-up crane vessel. The crane dynamics plays a less important role for blade

*Corresponding author

Email address: yuna.zhao@ntnu.no (Yuna Zhao)

installation by floating vessels, compared to the jack-up crane vessel. The floating vessels' wave-induced motion greatly affects the blade motion. The semi-submersible vessel causes a much smaller blade motion than the mono-hull vessel. The results indicate that it is feasible to install offshore wind turbine blades by using floating crane vessels provided that the vessel type is properly selected. From the operability point of view, semi-submersible vessels are more feasible than mono-hull vessels for offshore single blade installations.

Keywords: Offshore wind turbine blade installation, floating crane vessels, feasibility study, fully coupled method, dynamic motion response

1. Introduction

Installation of offshore wind turbines can be carried out by using either jack-up or floating crane vessels. The jack-up crane vessels are now extensively used during the installation of bottom-fixed offshore wind turbines (Ahn et al., 2017). They can provide a stable elevated working platform. Nevertheless, they are limited by water depth, deck space and jacking duration. They are significantly less competitive when it comes to intermediate water and deep water. Therefore, shortage of crane vessels remains a critical issue (Paterson et al., 2018) for installation of wind turbines in intermediate water and deep water.

At present, floating wind turbines experience rapid development due to the potential of much higher power production in deep water zones (Wind Europe, 2018). For floating wind turbines, it is only possible to use floating crane vessels if on site installation is inevitable, since use of jack-up crane

vessels is not feasible. The installation cost by floating crane vessels is usually much higher than that by jack-up crane vessels. When selecting the crane vessel in practical operations, technical feasibility and cost should be well balanced.

5 Compared to jack-up crane vessels, floating ones are flexible with respect to working water depth and fast in relocating. They are commonly used in the offshore oil and gas industry for installing sub-sea templates and topsides of platforms. At present, there are attempts of using floating crane vessels for offshore wind turbine installation, such as installing monopile foundations
10 for bottom-fixed wind turbines shown in Figure 1(a), installing the tower-rotor-nacelle assembly for floating wind turbines in Figure 1(b) and installing tower-nacelle assembly and rotor for floating wind turbines in Figure 1(c). Up to now, wind turbine blades have not been installed by using floating crane vessels.

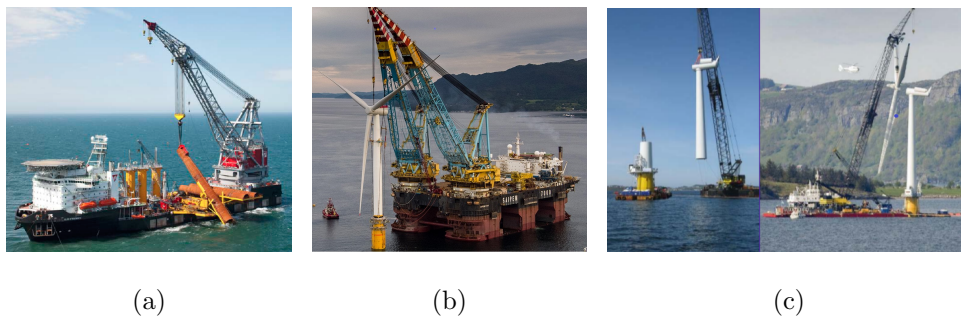


Figure 1: Examples of offshore wind turbine installation by using floating vessels. (a) installing a monopile for a bottom-fixed wind turbine by Oleg Strashnov, a mono-hull vessel (Seaway Heavy Lifting, 2018). (b) installing the tower and rotor-nacelle-assembly for a floating wind turbine by SAIPEM 7000, a semi-submersible vessel (Statoil, 2018). (c) installing tower-nacelle assembly (left) and rotor (right) for a floating wind turbine by a mono-hull vessel (Keseric, 2014).

There are studies on installation of offshore wind turbine components by floating cranes. Sarkar and Gudmestad (2013) proposed a method to install monopile foundations using a pre-installed submerged structure to isolate the foundation from the floating vessel motion. (Zhu et al., 2017) compared the dynamic motion response of a tripod foundation for offshore wind turbines during installation by a mono-hull and a jack-up crane vessel. Acero et al. (2017) studied the installation of an offshore wind turbine transition piece onto a monopile foundation by a mono-hull crane vessel. Ku and Roh (2015) studied the dynamic responses of an offshore wind turbine (tower-nacelle-rotor assembly) during lifting operation by a floating crane barge.

Installation of blades for offshore wind turbines is more challenging than other components (e.g. foundation, transition piece). This is because a high installation precision is required in the final blade mating phase and there is relative large motion between the turbine hub and the blade root at such large lifting height. Current industry practice is to use jack-up crane vessels to install offshore wind turbine blades. Jiang et al. (2018) studied the final mating phase of a 5MW wind turbine blade by a jack-up vessel onto a pre-assembled monopile and nacelle assembly. The blade root motion was found to be critical. The study found that the monopile hub motion can be important at certain wave periods when a resonant response is excited in the monopile. However, the blade root motion in this study is underestimated. Because it did not consider detailed modeling of the jack-up crane vessel, such as flexibility in jack-up legs and crane, jack-up leg soil-structure interaction and wave loads on jack-up legs, which are found to have significant influence on blade root motion during the final mating phase by Zhao et al. (2018b).

Compared to monopiles, the nacelle motions of typical jacket and tripod turbine foundations are much smaller (Shi et al., 2011). Therefore, for jacket and tripod wind turbines, the contribution of nacelle motion to the relative nacelle-blade root motion during blade mating is relatively small.

5 The present study aims at demonstrating the feasibility of offshore wind turbine blade installation by floating crane vessels. This is achieved by a detailed comparison of the blade dynamic motion response when installed by floating vessels with a representative jack-up crane vessel. Two different types of floating vessels are considered, i.e., a mono-hull and a semi-submersible
10 vessel. The focus is placed on the blade final mating phase, addressing the blade motion response. It is assumed that the turbine has a jacket foundation and the nacelle motion is relatively less important and not addressed in the present study.

Fully coupled time domain simulations are carried out using the SIMO-
15 RIFLEX-Aero code to study the dynamic responses of the three blade installation systems, including the motions of the vessel, crane tip, blade and blade root and tension in the tugger lines. The feasibility of using a floating vessel is demonstrated by showing that the motion and velocity of the blade root is within the limits experienced when a jack-up vessel is used. This approach
20 is believed to be conservative since the installation of a jack-up crane vessel itself is weather sensitive.

2. System description

Figures 2 shows the overall configuration of offshore single blade installation set-up by the semi-submersible, mono-hull and jack-up crane vessels,

respectively. An actual water depth of 39.1m is used in this study. Since bottom-fixed offshore wind turbines (e.g. monopiles) are more likely located in this water depth, and the motions of bottom-fixed offshore wind turbines are small, we neglected the motion of wind turbines during the numerical
5 analysis.

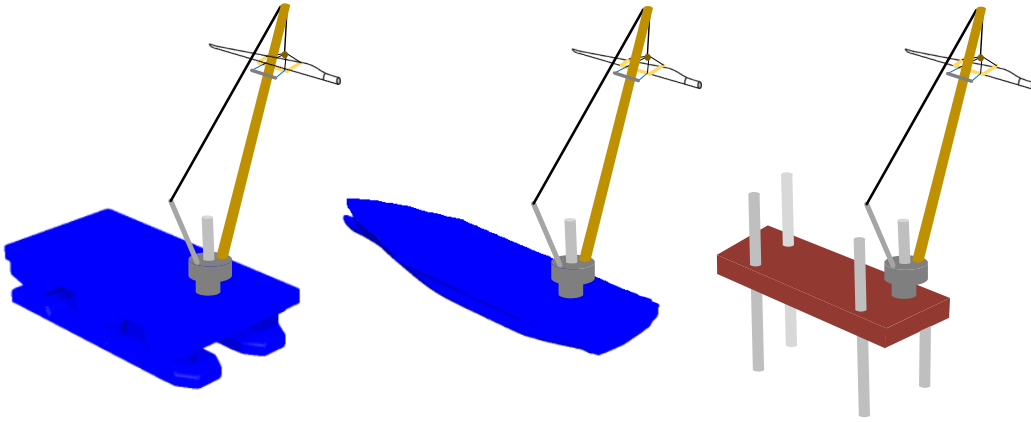


Figure 2: Offshore wind turbine installation using three different kinds of crane vessels: semi-submersible, mono-hull, jack-up.

The blade installation systems consist of three main parts, i.e., the vessel, the crane, and the installed blade and the lifting arrangements. Details of these three parts are provided in this section. The main properties of the three selected vessels are listed in Tables 1 and 2. The semi-submersible vessel
10 has two longitudinal pontoons that are completely submerged. The pontoons are connected to the main deck via six vertical columns. The displaced volume of the mono-hull vessel is about 40% of the semi-submersible vessel. Both the semi-submersible vessel and the mono-hull vessel are assumed to be equipped with dynamic positioning (DP) systems to keep the vessels in
15 position. The jack-up crane vessel has four legs with its hull elevated above

the mean sea surface during operations.

Table 1: Main parameters of the floating crane vessels

Parameters		Semi-submersible	Mono-hull
Length	[m]	175	183
Breadth	[m]	87	47
Operational draught	[m]	26.1	12
Displacement	[m^3]	1.638×10^5	6.190×10^4

Table 2: Main parameters of the jack-up crane vessel

Parameters	Unit	Values
Hull length, breadth and depth	[m]	132, 39, 9
Displacement during transportation	[m^3]	2.20×10^4
Total elevated load	[t]	1.69×10^4
Leg length and diameter	[m]	92.4, 4.5
Long. and trans. leg spacing	[m]	68.3, 30.6
Airgap	[m]	7.2
Leg below hull	[m]	49
Soil type		Dense sand
K_x, K_y and K_z *	[kN/m]	$1.35 \times 10^6, 1.35 \times 10^6, 1.47 \times 10^6$
K_ϕ, K_θ and K_ψ *	[kNm/deg]	$6.4 \times 10^5, 6.4 \times 10^5, 8.3 \times 10^5$

* Equivalent linear spring stiffness of the soil in the global coordinate system defined in Figure 4(c).

The same typical pedestal crane is used for all three crane vessels in this study, as shown in Figure 3. The pedestal crane consists of crane supports, a wire overhang system and a lattice boom. The crane is connected to the

vessel via the crane supports. In the numerical model, the boom is modeled using flexible beam elements with its lower end hinged on the crane base. The boom wires control the boom inclination and are represented by bar elements. The deformation of the crane supports, including king, pedestal and back-stay, is neglected (Zhao et al., 2018b). The main parameters of the crane are listed in Table 3.

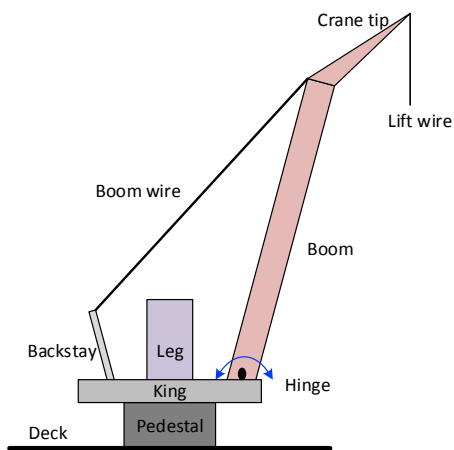


Figure 3: Illustration of a typical offshore pedestal crane (Zhao et al., 2018b)

The DTU 10 MW wind turbine blade (Bak et al., 2013) is used in this study. As shown in Figure 2, the blade is held by a yoke and lifted by the hook via four slings. The lift wire runs through the crane tip to the hook. Tugger lines are used for blade heading control which run from the yoke to a trolley on the crane boom. Pretension is applied in tugger lines to prevent slack lines. The main properties of the blade lifting system are summarized in Table 4.

As shown in Figure 4, three right-handed coordinate systems are defined and used for each blade installation system, i.e., a global coordinate system

Table 3: Main parameters of the crane

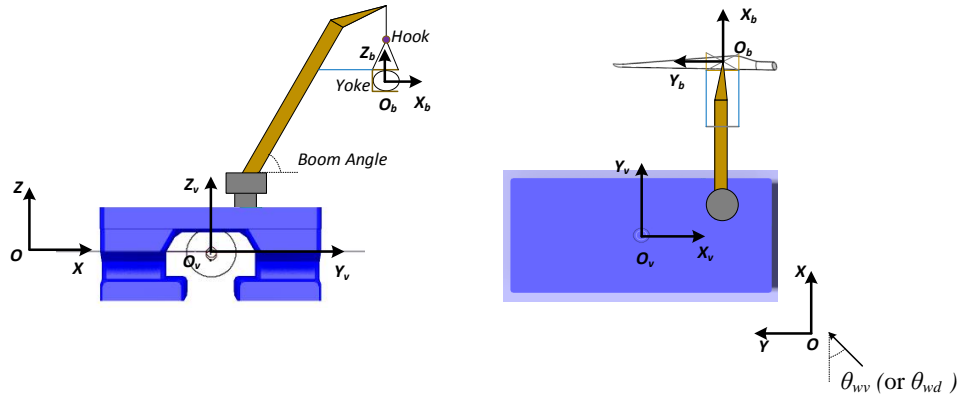
Crane properties (Zhao et al., 2018b)	
Boom length [m]	107.6
Crane boom angle [deg]	67.6
No. of equivalent boom wires [-]	2
Equivalent boom wire stiffness [kN/m]	9048
Equivalent boom wire damping [kNs/m]	90.5
Crane tip positions on the vessels *	
Semi-submersible vessel	(66m, 65.3m, 144.9m)
Mono-hull vessel	(74.2m,65.6m,144.9m)
Jack-up vessel	(34.2m,49.3m,133.2m)

* It is given in the vessel-related coordinate system. The height of crane tip on all three vessel are the same in the global coordinate system, i.e., 144.9m above the mean sea surface.

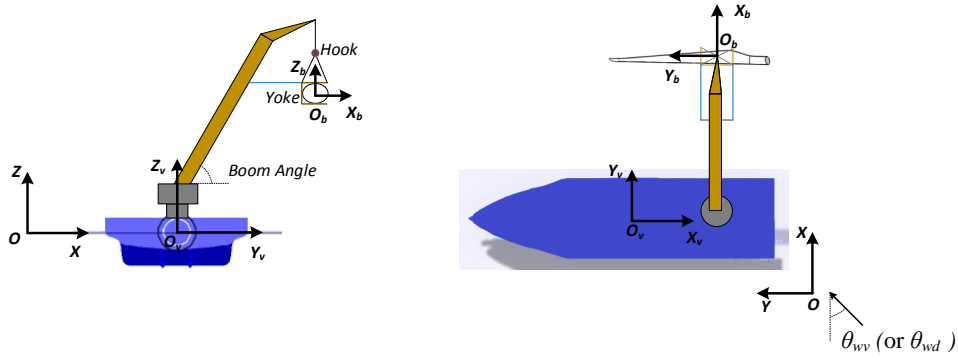
$O-XYZ$, a vessel-related coordinate system $O_v - X_v Y_v Z_v$ and a blade-related coordinate system $O_b - X_b Y_b Z_b$.

The blade-related coordinate system $O_b - X_b Y_b Z_b$ has its origin on the blade's center of gravity. Y_b is in the blade's longitudinal direction and is positive towards the blade tip; Z_b is positive upwards; X_b follows the right-hand rule. The $O_b - X_b Y_b Z_b$ parallels with the global coordinate system $O - XYZ$ when the blade is at rest.

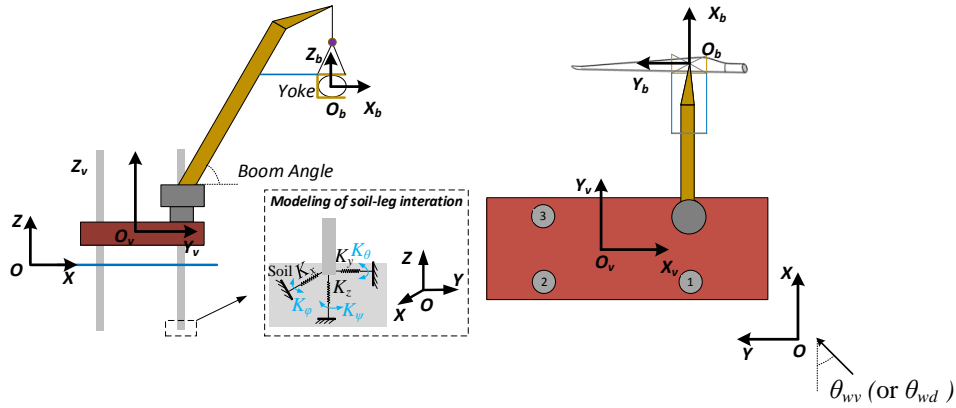
For the vessel-related coordinate system $O_v - X_v Y_v Z_v$, its origin is located at the center of the waterplane of the floating vessel at rest, while it sits on the geometrical center of the elevated jack-up hull. X_v is in the vessels' longitudinal direction and Z_v is positive upwards; Y_v follows the right-hand rule. When the vessel is at rest, $O_v - X_v Y_v Z_v$ will parallel with the global



(a) Semi-submersible vessel: side view and top view



(b) Mono-hull vessel: side view and top view



(c) Jack-up vessel: side view and top view

Figure 4: Definition of coordinate systems for the blade installation system: θ_{wv} is the incident wave angle while θ_{wd} is the wind inflow angle.

Table 4: Main properties of the blade and the lifting arrangement (Zhao et al., 2018a)

Parameter	Value
Hook mass [tons]	10
Yoke mass [tons]	47
Blade mass [tons]	41.67
Blade length [m]	86.37
Installation height [m]	119
Length of crane wire (from crane tip to hook) [m]	4.7
Length of slings [m]	20.4
Tugger line arm length (relative to blade COG) [m]	10
Length of tugger line [m]	5.7
Stiffness of tugger line [kN/m]	525

coordinate system $O - XYZ$ if it rotates around the Z_v axis by 90 deg.

The global coordinate system $O - XYZ$ has its origin located at the mean sea surface. Z is positive upwards. X parallels with the Y_v when the vessels are at rest. The Y follows the right hand rule.

5 The incident wave angle, i.e., θ_{wv} , is defined as the relative angle of wave direction and the positive X direction in the global coordinate system. The incident wind angle θ_{wd} has a similar definition while the wind and waves do not always have the same incident angle.

3. Methodology

10 The fully coupled code, the SIMO-RIFLEX-Aero (Zhao et al., 2018b) is used to conduct the integrated dynamic analysis of single blade installation by three crane vessels in time domain. The coupled code is an integration of three programs, i.e., SIMO (SINTEF Ocean, 2017b), RIFLEX (SINTEF

Ocean, 2017a) and Aero (Zhao et al., 2018a). Detailed structural models for the blade installation systems are shown in Table 5.

Table 5: Structural model for the blade installation systems

Component	Modeling
Blade	Rigid body with 6 DOFs in SIMO
Hook	Point mass at the lower end of lift wire in RIFLEX
Boom wire, lift wire and slings	Bar elements in RIFLEX
Tugger lines	Bi-linear springs (only tension, no compression) in SIMO
Crane boom	Beam elements with circular cross-section, hinged at the lower end in RIFLEX
Crane base	Rigid (master slave connections between the nodes) in RIFLEX
Jack-up hull	Rigid body with 6 DOFs in SIMO
Jack-up hull-leg connections	Rigid
Jack-up legs	Beam elements with ring cross-sections in RIFLEX
Jack-up soil-structure interaction	Linear springs and dampers in 6 DOFs at the lower ends of all legs in RIFLEX
Floating vessels	Rigid bodies with 6 DOFs in SIMO

The external force models for the blade installation systems are presented in Table 6. The aerodynamic loads acting on the installed blade are computed in the Aero code based on the cross-flow principle (Horner, 1965; Hoerner and Borst, 1985). At each time step, the Aero code calculates the aerodynamic loads using the instantaneous blade position provided by SIMO and the relative wind velocity seen by the blade. The aerodynamic loads are then imported by SIMO (Zhao et al., 2018a).

The hydrodynamic load modeling for the jack-up vessel and the floating vessels are different, as shown in Table 6. The hydrodynamic loads on the jack-up legs are calculated based on the Morison’s formula (diameter to wave length ration $< 1/5$), with integration to the instantaneous sea surface considering the presence of water inside the legs (Zhao et al., 2018b).

For the floating vessels, the hydrodynamics loads are calculated based on

Table 6: External force model for the blade installation systems

Component	Force model
Blade	Aerodynamic load calculated in the Aero code, including influence of wind shear, wind turbulence and dynamic stall
Jack-up hull	Wind loads with equivalent wind area and wind coefficients
Jack-up legs	Hydrodynamic loads calculated using Morison's formula with integration to the instantaneous sea surface considering water inside the legs
Floating vessels	Hydrodynamic loads calculated by using the 1st and 2nd order potential theory considering viscous roll damping; dynamic forces from the DP systems are modeled as equivalent linear stiffness terms with 70% of critical damping in surge, sway and yaw

the potential flow theory. The hydrostatic restoring coefficients are computed using the mean position of the vessels. The added mass, potential damping and first order wave excitation forces are obtained using a first order potential flow model and applied in the time domain using the convolution techniques (SINTEF Ocean, 2017b). Additional viscous roll damping is incorporated as 3% of the vessel's critical damping in roll (Pedersen, 2012). In addition to the first order hydrodynamic forces, the mean wave drift loads are also considered. The Newman's approximation is used to estimate the second order difference frequency wave excitation loads on the mono-hull vessel in surge, sway and yaw. For the semi-submersible vessel, integration of second order mean wave pressure over its wetted surface is used to estimate the second order difference frequency wave excitation forces in all 6 DOFs, as recommended in the DNV-RP-C205 guideline (DNV, 2007). The restoring forces of the DP system are simplified into equivalent linear stiffness terms in surge, sway and yaw. Besides, large damping, i.e., 70% of the critical damping of the vessels' surge, sway and yaw motion, is applied to eliminate the

corresponding slowly varying motion. This is a reasonable assumption since it can be achieved by use of DP systems in practical operations (SINTEF Ocean, 2017c).

4. Identification of system natural periods

5 The natural periods of the three blade installation systems are estimated in this section. Since the blade installation systems are complex, the natural periods are identified module by module.

4.1. Vessels

Eigenvalue analyses are conducted to identify the natural periods of the
10 vessels' motion, excluding the crane and blade.

For the floating vessels, their natural frequencies are obtained by solving Eq.(1).

$$[-\omega^2(\mathbf{M} + \mathbf{A}_\infty) + \mathbf{K}] \cdot \mathbf{x} = 0 \quad (1)$$

where \mathbf{M} is the vessel mass matrix; \mathbf{A}_∞ is the added mass matrix at infinite frequency; \mathbf{K} is the restoring matrix which is the sum of the hydrostatic
15 restoring and the equivalent restoring from the DP system.

The eigenvalue analysis for the jack-up vessel is solved by using the Lanczos method (SINTEF Ocean, 2017a), considering the flexibilities in the jack-up legs and the soil foundations.

The results are presented in Table 7. The natural periods of the semi-
20 submersible vessel are above 18s. The natural periods of the mono-hull vessel motion in heave, roll and pitch are between 9s~14s, which are within typical

wave period range. The natural periods of the jack-up vessel motion are much shorter than those of the two floating vessels.

Table 7: Natural periods of vessels' motions (defined in the vessel-related coordinate systems in Figure 4)

Vessel	Surge	Sway	Heave	Roll	Pitch	Yaw
Semi-submersible	83.68 s	75.29 s	22.64 s	23.56 s	18.20 s	86.72 s
Mono-hull	87.27 s	75.23 s	10.00 s	13.51 s	9.07 s	85.69 s
Jack-up	2.912 s	3.087 s	2.363 s	0.479 s	0.594 s	0.451 s

4.2. Crane

The crane boom is hinged at its lower end, The crane motion is mainly
 5 caused by the deformation of the boom wires. The natural period of the crane motion is identified by conducting decay tests while the vessel is fixed. In the current blade installation scenario, the crane motion has a natural period of 2.9s.

4.3. Blade

10 The natural frequencies of blade rigid body motion are obtained by eigenvalue analysis, together with the hook while keeping the vessel and the crane fixed, based on Eq.(1). Since the blade and the hook are in air, the corresponding added mass matrix \mathbf{A}_∞ is neglected. The restoring matrix \mathbf{K} is mainly resulted from the mechanical wire coupling forces from the lift wire,
 15 slings and tugger lines.

The dominant motions of the blade rigid body motion and corresponding periods and frequencies are listed in Table 8. The blade-hook in-phase pendulum motion has the longest natural period of 12s, followed by the blade

Table 8: Natural periods and dominant motion of the blade motion (defined in the blade-related coordinate systems in Figure 4)

Dominant response	Period [s]	Frequency [rad/s]
Blade roll resonance (in phase pendulum motion)	12.0	0.52
Blade yaw resonance (due to tugger lines)	5.11	1.23
Blade-hook double pendulum around the crane tip in the $O_b - Y_b Z_b$ plane (blade and hook motion out of phase)	3.63	1.73
Blade surge resonance (due to tugger lines)	1.90	3.31

yaw resonant motion with a period around 5s. The third mode is caused by the out-of-phase double pendulum motion of the blade and hook around the crane tip in the vertical $O_b Y_b Z_b$ plane (Zhao et al., 2018a). The natural period of blade surge motion due to tugger line restoring effects is around
5 1.9 s. As a result, the blade surge resonance is generally not excited.

5. Load cases and environmental conditions

A series of load cases (LCs) are defined for the blade installation systems and used in the time domain simulations, as shown in Table 9. LC1 is a turbulent wind only case. LC2 is an irregular wave only case. They are used
10 to formulate a comparison against LC3 to reveal the influence of wind and waves on the system dynamic responses.

LC3~LC7 have correlated turbulent wind and irregular waves. In these load cases, the significant wave height and peak period are correlated with the mean wind speed. The correlation is based on the measurement and
15 analysis of data obtained at the North Sea Center site (Li et al., 2015). The wind turbulence intensity is calculated according to the IEC class A, which is the design class for the DTU 10MW wind turbine (Bak et al., 2013). The

Table 9: Load cases: turbulent wind and irregular waves

LC	U_w [m/s]	T_I [%]	H_s [m]	T_p [s]	θ_{wd} [deg]	θ_{wv} [deg]	Sim. length [s]
LC1	7.0	24.8	-	-	0	-	3600×5
LC2	-	-	1.0	7.3	-	0	3600×5
LC3	7.0	24.8	1.0	7.3	0	0	3600×5
LC4	7.0	24.8	1.0	7.3	0	315	3600×5
LC5	7.0	24.8	1.0	7.3	0	270	3600×5
LC6	8.3	22.9	1.5	7.7	0	0	3600×5
LC7	5.6	28.0	0.5	6.8	0	0	3600×5
LC8	7.0	24.8	1.0	[5,6,7,8,9,10]	0	285	6×(3600×5)

U_w - mean wind speed; T_I - turbulence intensity factor; θ_{wd} - wind inflow angle; θ_{wv} - wave incident angle; $\theta_{wv} = 0^\circ$ - beam sea; $\theta_{wv} = 315^\circ$ - quarter sea; $\theta_{wv} = 270^\circ$ - head sea.

wave direction is varied in LC3~LC5, i.e., beam sea, quarter sea and head sea, to study the impacts of misalignment of wind and wave on the system motion responses. LC6 and LC7 are two correlated wind and wave conditions that are different from LC3. They are used to identify the dynamic response characteristics of system under various sea states.

A parametric study is carried out in LC8, to further investigate the effect of wave peak period on the performance of floating crane vessels. The wave peak period varies from 5s to 10s, while the significant wave height and wind condition are kept the same as LC3. The wave direction in LC8 is assumed to be 285 deg, close to the vessel head sea direction to utilize the wave orientation to improve vessel performance. The 15 deg offset from the head sea direction is recommended by DNV-RP-H103 (DNV, 2014) to represent a practical head sea condition during operation.

During the simulations, the turbulent wind field is generated by using the TurbSim code (Jonkman, 2009) according to the Kaimal turbulence model.

The irregular waves are long crested and are modeled by using the JONSWAP spectrum with $\gamma = 1$ (DNV, 2007).

Five identical and independent simulations are carried out for each load case. Each simulation lasts for one hour after removing the start-up transient part. The statistical values and power spectra of the dynamic motion
5 responses presented in the next section are obtained based on the average of five one-hour simulations.

6. Results and discussion

6.1. Hydrodynamic performance of the floating vessels

10 Prior to the comparative study of the dynamic responses of the three blade installation systems, the hydrodynamic properties of the two floating vessels are investigated. Their hydrodynamic coefficients, i.e., the added mass, potential damping, first order wave excitation force transfer function and first order motion transfer function, are calculated in frequency domain.
15 The water depth considered is 39.1m. The results in vessel roll (ϕ_v) are shown in Figure 5. The former three are non-dimensionalized using the following definitions:

- A_{44} is non-dimensionalized by $\rho V L^2$.
- B_{44} is non-dimensionalized by $\rho V L \sqrt{gL}$.
- 20 • H_4^1 is non-dimensionalized by $\rho V g A_{wave}$.

where ρ is the water density; V is the vessel displaced volume; L is the vessel length; g is the acceleration of gravity; A_{wave} is the unit wave height.

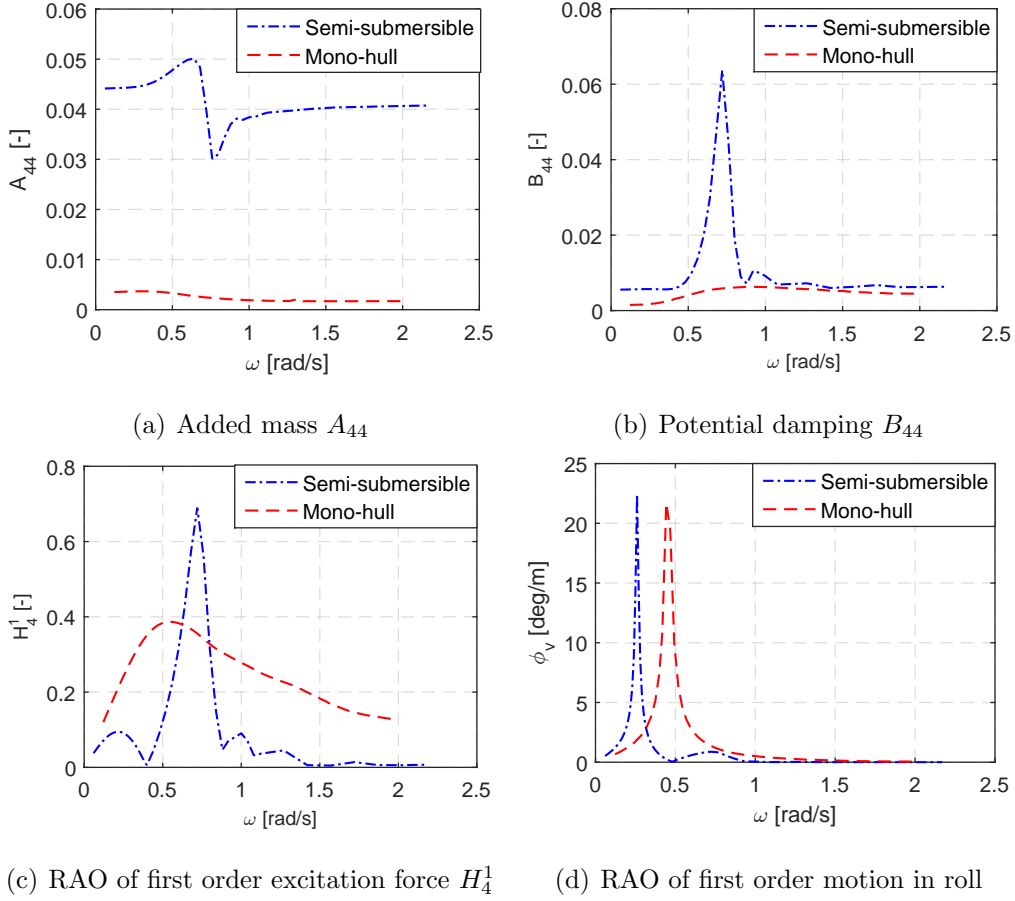


Figure 5: Non-dimensional added mass, potential damping and transfer function of the first order wave excitation force and motion of the floating vessels in roll. The transfer functions of first order wave excitation force and first order motion are estimated with incident wave angle of 0° . It should be noted that the RAO of wave excitation force, rather than the motion RAO is used in the time domain analysis. The RAO of vessel roll motion shown here just aims to illustrate the variation of vessel motion with incident wave period.

The layout of the semi-submersible vessel contributes to a large added mass coefficient in roll, i.e., A_{44} , which is larger than the corresponding mass moment of inertia I_{44} . For the mono-hull vessel, its A_{44} is less than 20% of

its I_{44} .

The RAO of the first order wave excitation force H_4^1 of the semi-submersible vessel is overall smaller than the mono-hull vessel. Even though the former exceeds the latter in the frequency range of 0.65~0.75 rad/s (by less than 5 50%). The large added mass and potential damping of the former help to limit its dynamic response. Overall, the former has better hydrodynamic performance than the latter within typical wave frequency range, as shown in Figure 5(d).

6.2. Characteristics of system motion responses

10 The system dynamic motion characteristics are discussed in this section based on the time domain simulation results, including the vessel motion (6 DOFs) and the crane tip motion (3 DOFs) in the vessel-related coordinate systems, and the blade motion (6 DOFs) and the blade root motion (3 DOFs) in the blade-related coordinate systems. The standard deviations of positions 15 of the crane tip, the blade center of gravity and the blade root are compared in the global coordinate system.

6.2.1. Vessels

The standard deviations of the vessel motion in LC1~LC7 are presented in Figure 6.

20 The vessel motions are mainly wave-induced, as indicated by the comparisons among LC1, LC2 and LC3. Compared to the jack-up vessel, the floating vessels have larger motions in all 6 DOFs. The semi-submersible vessel has smaller motions than the mono-hull, due to its better hydrodynamic performance as discussed in Section 6.1.

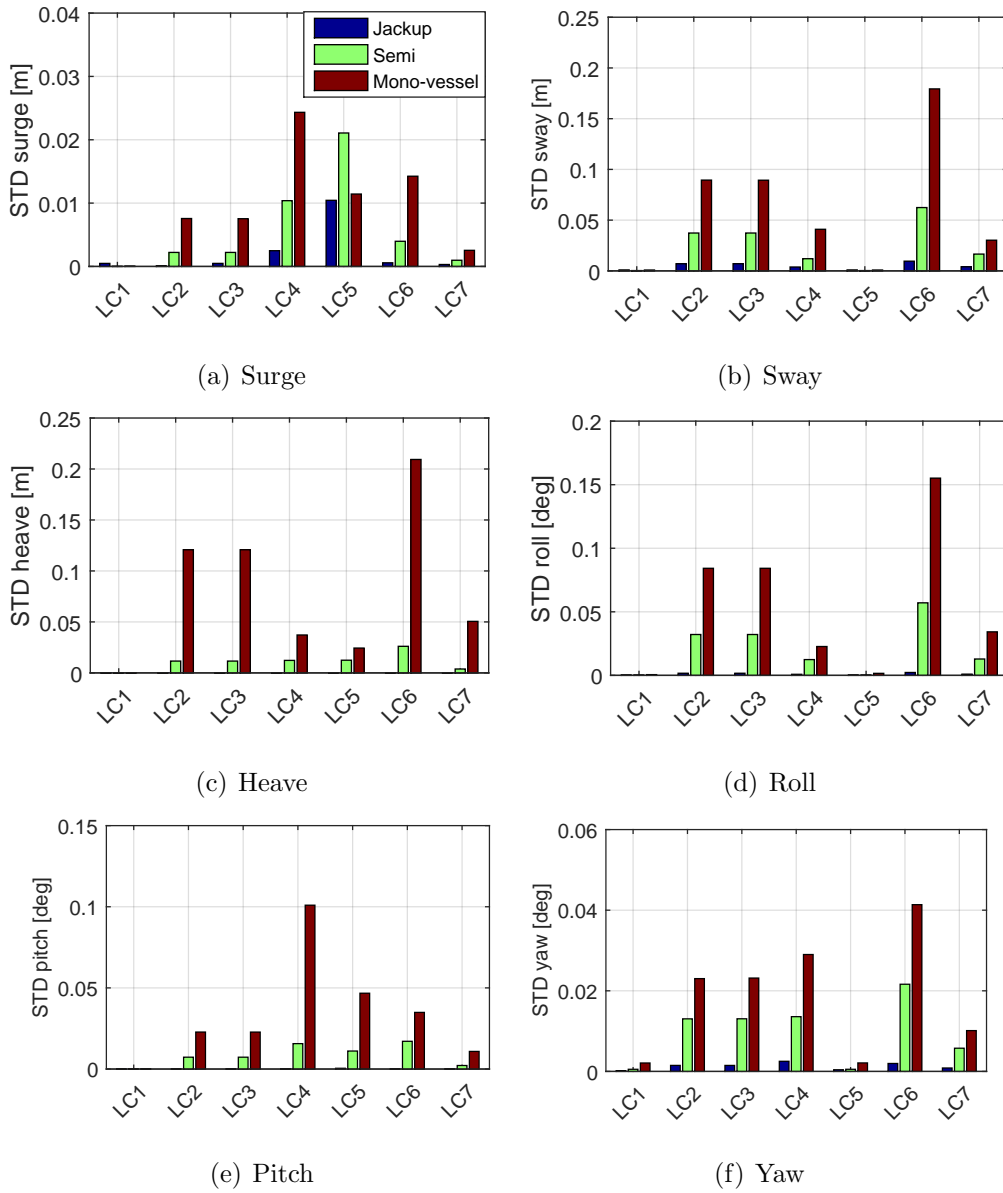


Figure 6: Standard deviations of vessel motion in LC1~LC7 in the vessel-related coordinate system.

The power spectra of vessel motion in sway and roll in LC3 are shown in Figure 7. The jack-up vessel has minor wave frequency response and

is dominated by the vessel sway resonant motion. The mono-hull vessel's sway motion experiences a large contribution from the slowly varying sway motion, which is dominant in short waves. For both of the floating vessels, the wave frequency response is found to be significant, especially in roll motion, as shown in Figure 7(b). The mono-hull vessel roll motion has its natural period close to the wave peak period and hence gets significant wave load excitations, leading to large wave frequency response. The mono-hull vessel's motion in heave and pitch has a similar trend.

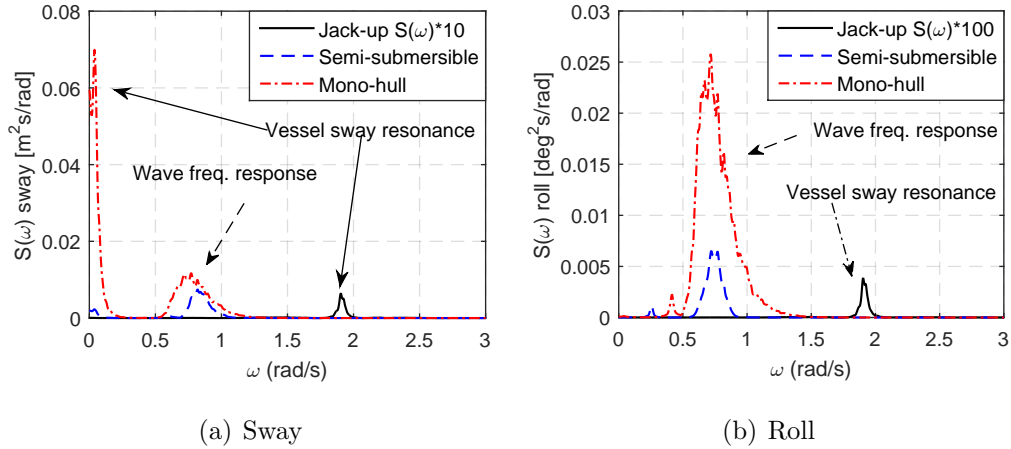


Figure 7: Power spectra of vessel motion in LC3

6.2.2. Crane tip

The crane tip motion is given in the vessel-related coordinate system. Its standard deviations are shown in Figure 8.

For crane operations at large lifting height, the vessel's rotational motion greatly contributes to the crane tip motion. As a result, the amplitude of crane tip motion is generally larger than the vessel translational motion, which can be observed by comparing Figures 6(a) and 8(a), and by comparing

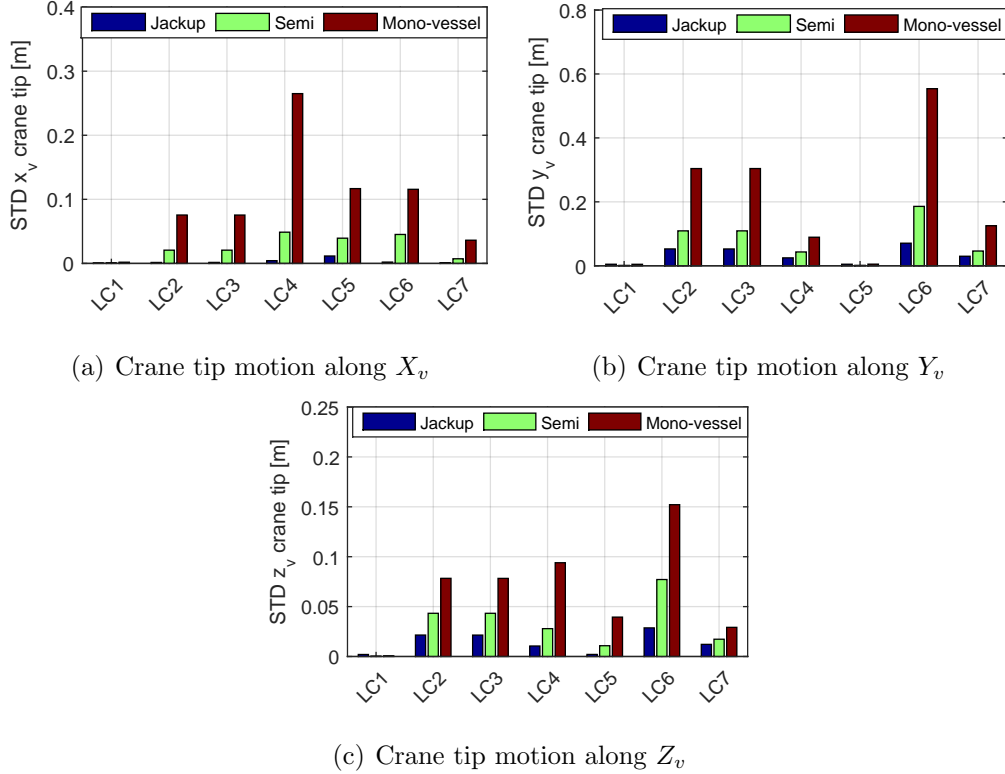
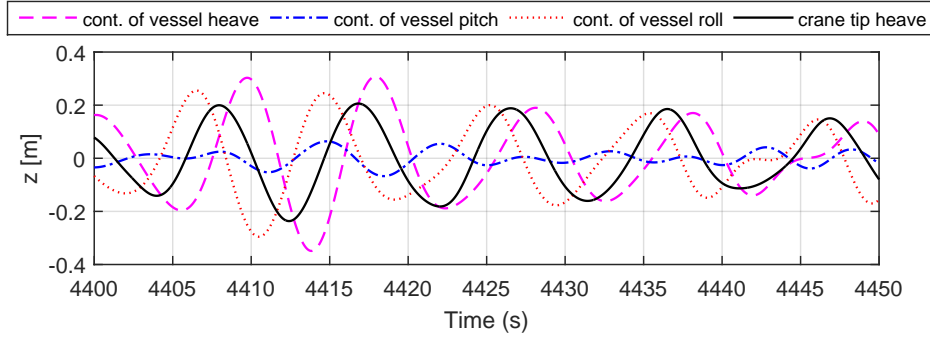
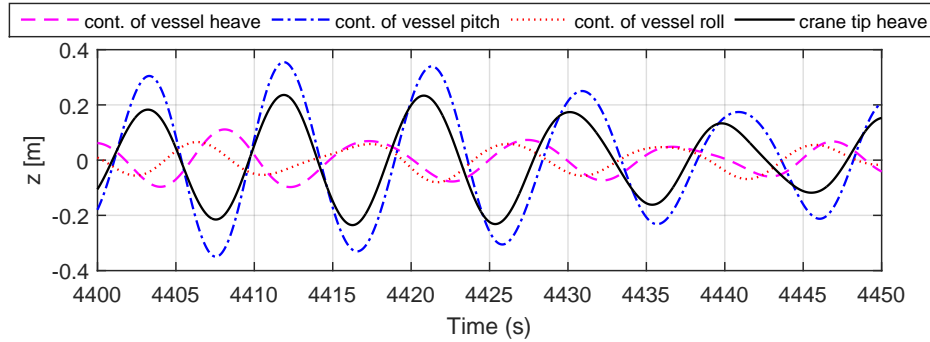


Figure 8: Standard deviations of crane tip motion in LC1~LC7 in the vessel-related coordinate system.

6(b) and 8(b), respectively. However, the former can be smaller than the latter in some cases. For example, the crane tip motion in Z_v direction (in the vessel-related coordinate system) is smaller than the vessel heave motion for the mono-hull vessel in LC3, LC6 and LC7, as can be found by comparing Figures 6(c) and 8(c). The corresponding time series in LC3 are further analyzed, as shown in Figure 9(a). The contributions of the mono-hull vessel's heave and roll motions dominate the crane tip motion in Z_v direction in LC3. The contribution from vessel roll motion is out of phase with that of vessel heave motion, resulting in the crane tip motion in Z_v



(a) LC3



(b) LC4

Figure 9: Contributions of mono-hull vessel's motion to the crane tip motion in Z_v direction in the vessel-related coordinate system in LC3 and LC4.

direction smaller than the vessel heave motion. In LC4, the vessel pitch is remarkable. It has much larger contribution to the crane tip motion in Z_v direction than vessel heave and roll motions, as shown in Figure 9(b). As a result, the crane tip motion in Z_v direction has a larger amplitude than the vessel heave motion.

Overall, the crane tip on the jack-up vessel has the smallest motion, followed by that on the semi-submersible vessel and that on the mono-hull vessel. Spectral analysis is carried out to further identify the differences. As

shown in Figure 10, the crane tip motion on the floating vessels is highly dominated by the wave frequency response due to floating vessels' motion. The motion contribution from the crane movement caused by crane elastic deformation is relatively less important on the floating vessels. Nevertheless, it has a notable contribution for the crane tip motion on the jack-up crane vessel, as shown in Figure 10(b).

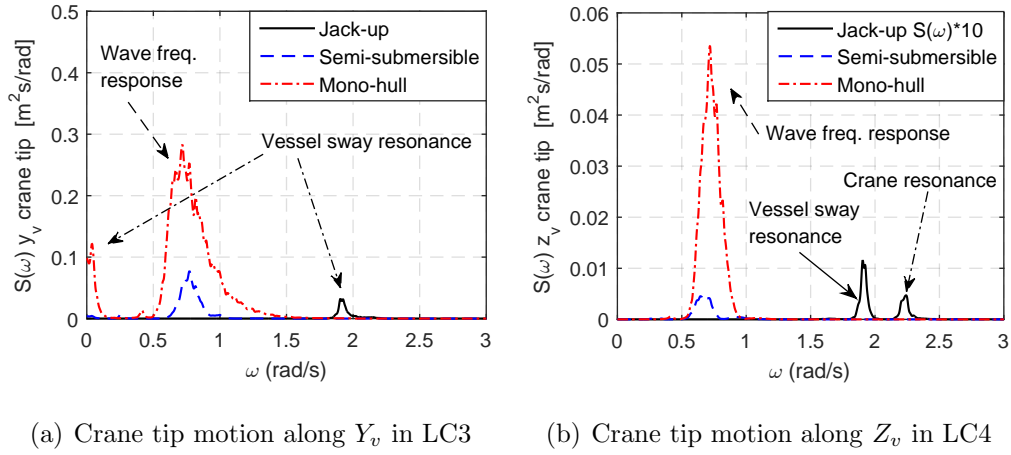


Figure 10: Power spectra of crane tip motion in LC3 and LC4 in the vessel-related coordinate system.

Similar to the vessel motion, the dynamic responses of the crane tip are sensitive to the variations in wave conditions, as can be found by comparing LC3~LC7 in Figure 8. Comparison among LC3, LC6 and LC7 shows that the crane tip motion increases significantly with increasing wave height. The crane tip motion along X_v has the maximum response in LC4 with quartering sea. The crane tip motions along Y_v and Z_v reach their maximum values in LC5 with head sea. It shows that the crane tip motion can be reduced by adjusting the vessel heading relative to the wave direction.

6.2.3. Blade

The standard deviations of the blade motion in the blade-related coordinate system are presented in Figure 11.

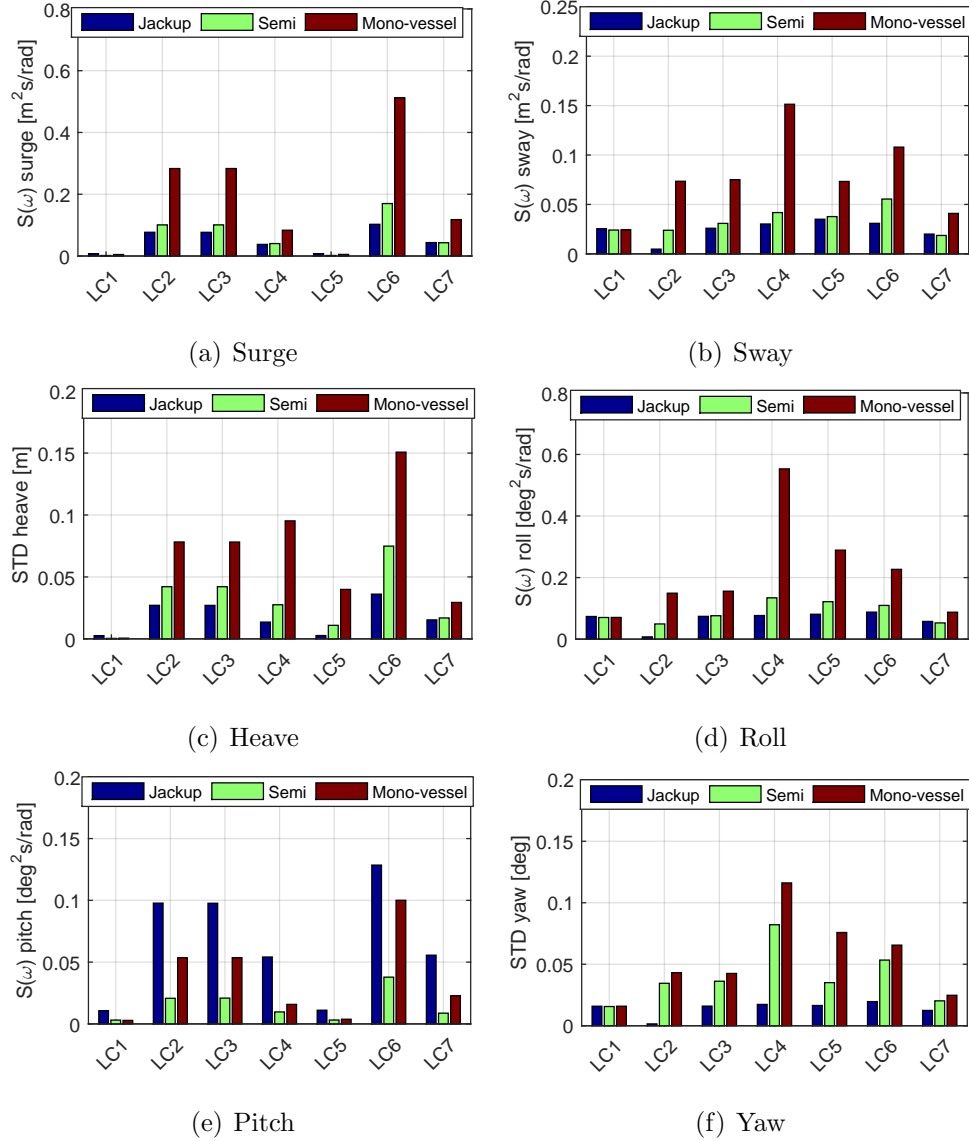


Figure 11: Standard deviations of blade motion in LC1~LC7 in the blade-related coordinate system.

Comparisons among LC1~LC3 show the relative importance of wave-induced vessel motion and blade aerodynamic loads in the blade dynamic response. The former is the main contributor to the blade motion in surge, heave and pitch. The blade motion in other DOFs shows remarkable dependency on both of them. Nevertheless, their relative contribution varies from vessel to vessel, as shown in Figure 12. For the jack-up vessel, the blade roll motion is mainly induced by the blade aerodynamic loads. When installed by the floating vessels, the blade roll motion is also affected by the vessels' wave-induced motion. For the semi-submersible vessel, the wave frequency response is slightly excited. The wave frequency response is remarkable for the mono-hull vessel and as a result, the double-pendulum motion is excited. Overall, the effect of wave-induced vessel motion dominates over that of the aerodynamic loads in blade roll motion for the mono-hull vessel, as can be observed in Figures 11(d) and 12(c). A similar trend exists for the blade motion in sway on the mono-hull vessel.

The contribution of wave-induced vessel response in the blade dynamic motion experiences a significant variation under different wave conditions, which is revealed by comparing the results of LC3~LC7 in Figure 11. The maximum contributions from the wave frequency responses are seen in LC6 which is the severest sea state within LC1~LC7. The amplitudes of blade motion are dependent on the wave direction. The blade surge, heave and pitch motions reach their minimum values in head sea condition in LC5, as shown in Figure 11. The blade motion in sway, roll and yaw reaches minimum in beam sea in LC3 and maximum in quartering sea in LC4. The

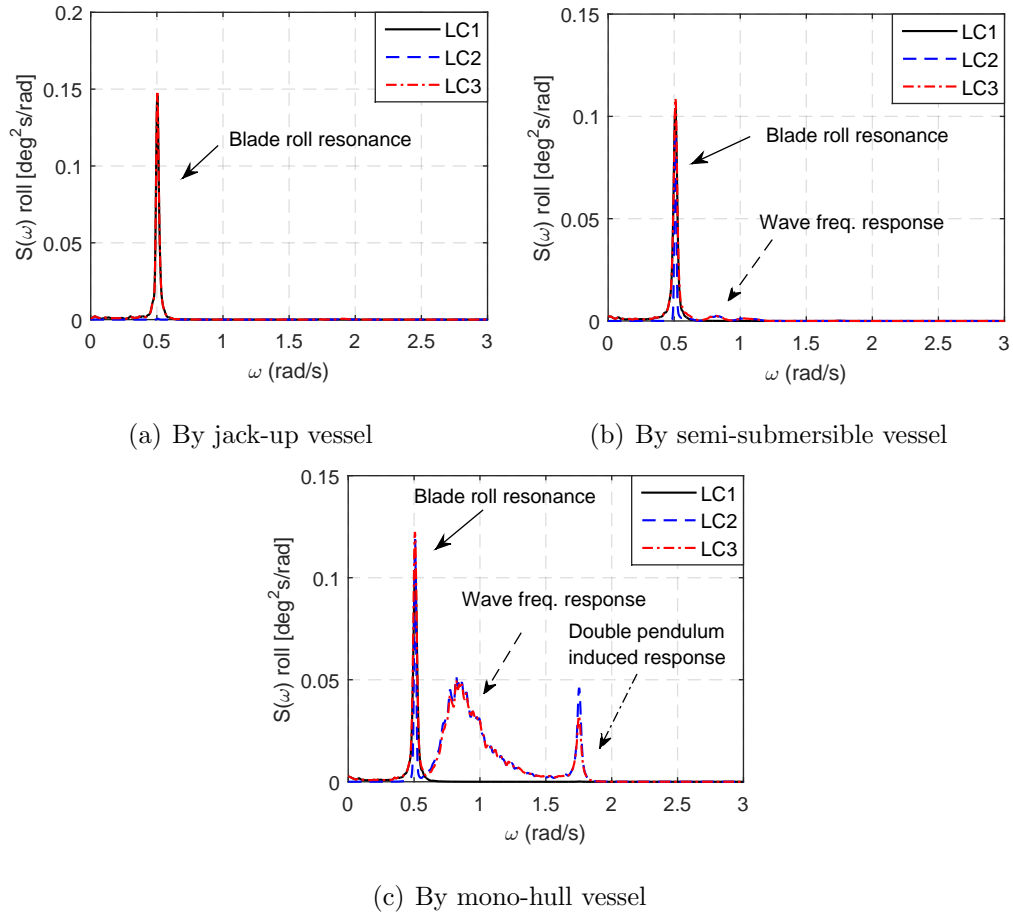


Figure 12: Power spectra of blade roll motion in LC1~LC3

power spectra of the blade yaw motion in LC3~LC5 are presented in Figure 13. The blade yaw motion on the semi-submersible vessel has a relatively small contribution from the wave-frequency response. It is mainly dominated by the blade yaw resonant motion which is significantly excited in quartering sea in LC4. On the mono-hull vessel, the blade yaw motion also has a remarkable contribution from the wave frequency response. It excites the blade roll resonance as well in LC4 and leads to a large increase in blade yaw

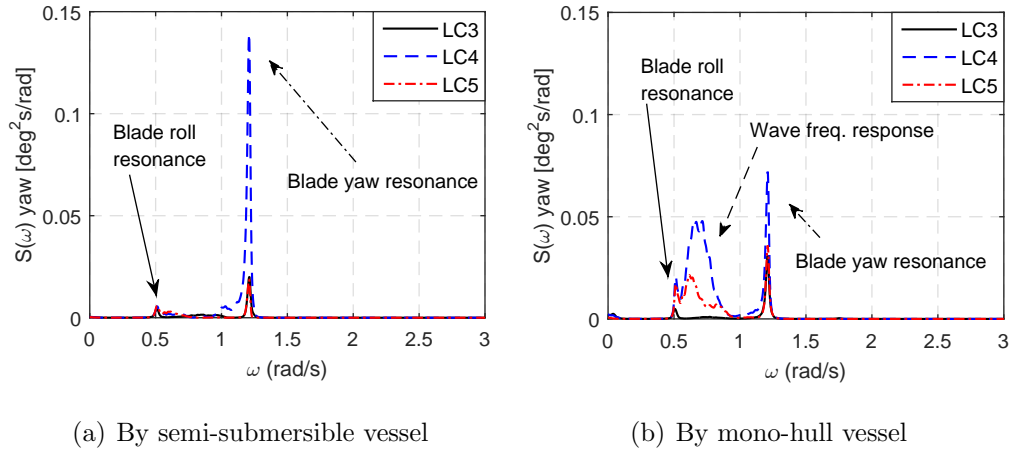


Figure 13: Power spectra of blade yaw motion in LC3~LC5

motion.

Similar to the crane tip motion, the blade motion on the floating vessels has relatively less important contributions from the crane dynamics, as shown in Figure 14. On the jack-up vessel, the crane resonant response is important for the blade motion because it is excited by the jack-up vessel motion since their natural periods are very close.

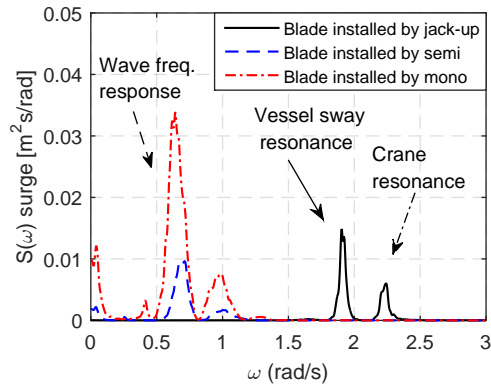


Figure 14: Power spectra of blade surge motion in LC4

6.2.4. Blade root

The dynamic motion at the blade root is critical for the mating process of blade root into the turbine hub. The blade root motion is given in the blade-related coordinate system. The standard deviations of blade root motion are shown in Figure 15.

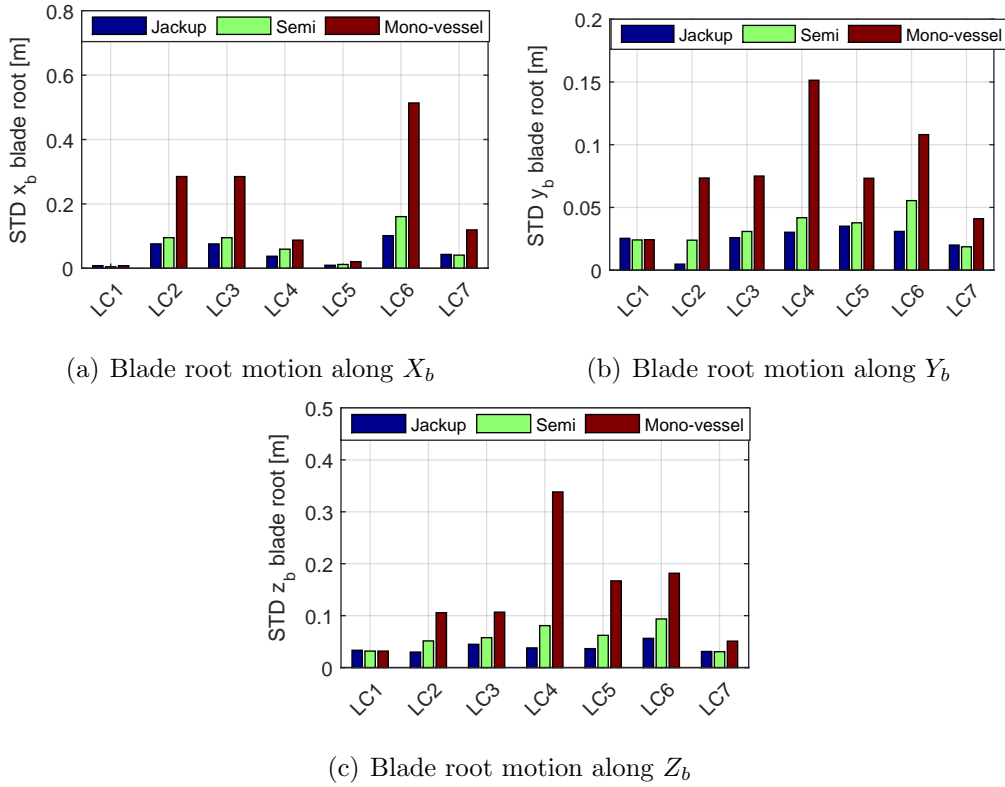


Figure 15: Standard deviations of blade root motion in LC1~LC7 in the blade-related coordinate system.

The blade root motion along X_b is mainly resulted from the blade surge and yaw motions. The latter has very limited contribution since it is well controlled by the tugger lines. The blade root motion along Y_b is mainly caused by the blade sway; thus, their dynamic characteristics are similar. The

blade root motion along Z_b is a result of the blade heave and roll motions. It has larger amplitudes than the blade heave motion because of the significant contribution from the blade roll motion.

The blade root motion is affected by both wind and wave loads, as indicated by the comparison among LC1~LC3, and LC3~LC7 in Figure 15. Figure 16 shows the power spectra of blade root motion in X_b and Z_b in LC3. The blade root motion along X_b has significant wave frequency response for the floating vessels, as shown in Figure 16(a); it is thus sensitive to the wave condition. The blade root motion along Z_b shows significant dependency on blade motion caused by both aerodynamic loads and wave-induced vessel motion, which can be observed in Figure 16(b). Hence it is sensitive to both wind and wave conditions.

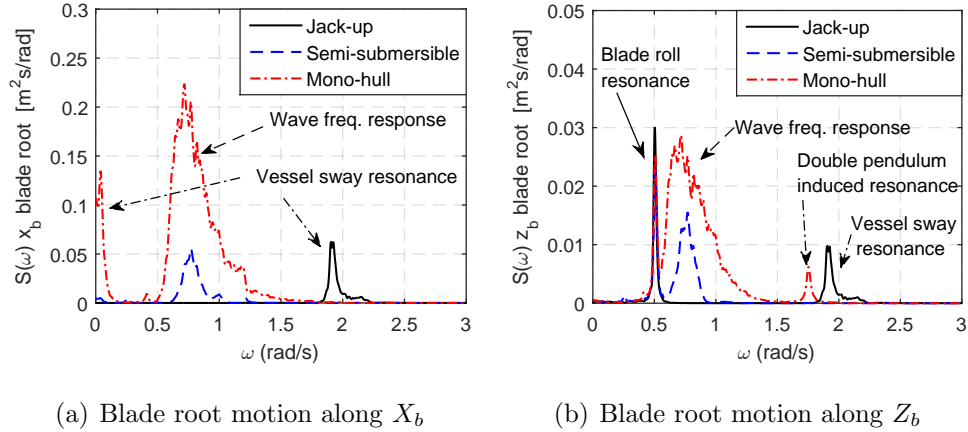


Figure 16: Power spectra of blade root motion along X_b and Z_b in the blade-related coordinate system in LC3

Compared with the semi-submersible vessel, the blade root motion on the mono-hull vessel is much larger and shows more significant variations with changing wave conditions, which can be found by comparisons within

LC3~LC7 in Figure 15. Because it has much more contributions from the wave-frequency response caused by vessel motion since the mono-hull vessel gets larger wave load excitation due to its hydrodynamic properties, as shown in Figure 16. The power spectra of blade root motion along Y_b on the mono-hull and the semi-submersible vessels in LC3, LC6 and LC7 are compared in Figure 17. The blade root motion along Y_b on the mono-hull vessel has significant wave frequency response which increases dramatically from LC7, LC3 to LC6. For the semi-submersible vessel, the blade root motion along Y_b has much less contribution from the wave-induced vessel motion and thus has a lower amplitude.

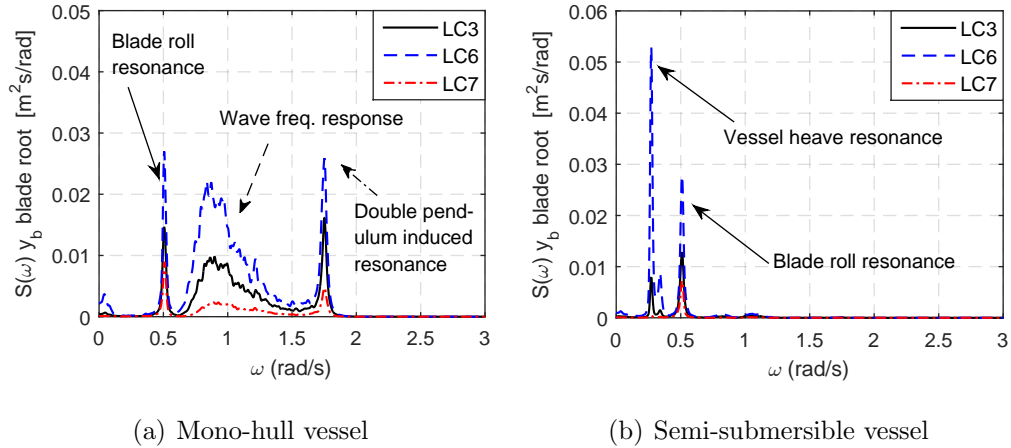


Figure 17: Power spectra of blade root motion along Y_b in the blade-related coordinate system for the mono-hull and semi-submersible vessels in LC3, LC6 and LC7

6.2.5. Effect of wave period on blade root motion

Figure 18 shows the standard deviations of the blade root motion in the blade-related coordinate system in LC8 with varying wave peak period (5~10s). By taking advantage of the vessel weather orientation, the ampli-

tudes of blade root motion along X_b in LC8 with $T_p = 7s$ are greatly reduced, compared to LC3.

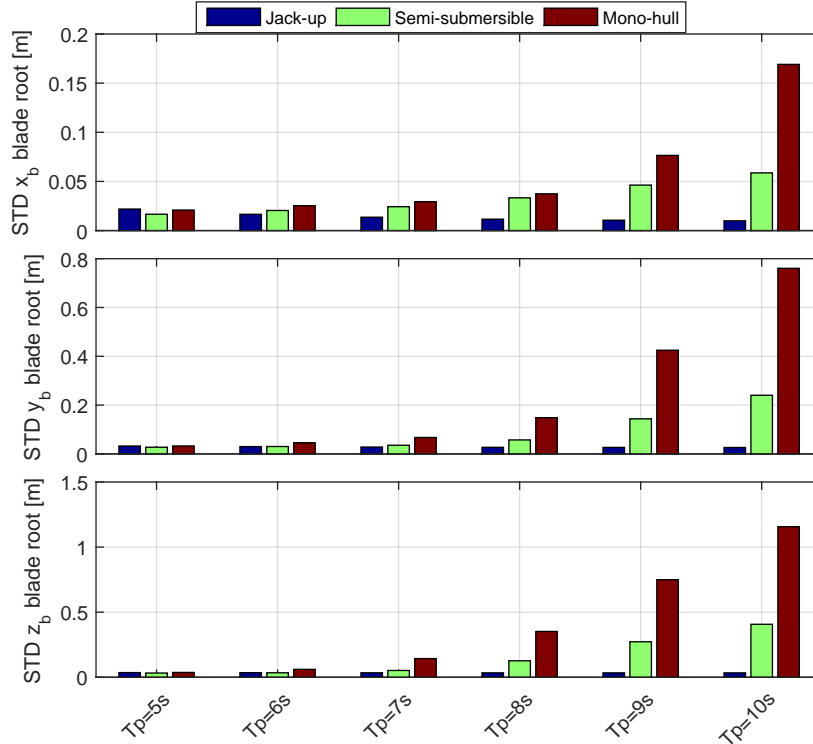


Figure 18: Standard deviations of blade root motion in the blade-related coordinate system in LC8 with varying wave peak period.

As can be observed in Figure 18, the root motion of the blade installed by the jack-up crane vessel decreases with the increasing wave peak period. Because the vessel gets less wave load excitations as the wave peak period shifts further away from the natural periods of vessel motion. On the contrary, the blade root motion increases significantly on the floating crane vessels. The mono-hull vessel causes the largest increase in blade root motion, since the vessel motion in the vertical plane is highly excited with the increasing wave

peak period. Compared to the mono-hull vessel, the semi-submersible vessel causes a much smaller increase in blade root motion, since its motion natural periods are much larger than the wave periods considered. The results indicate that a floating vessel with motion natural frequencies far from typical wave frequency range helps reduce the blade root motion during installation.

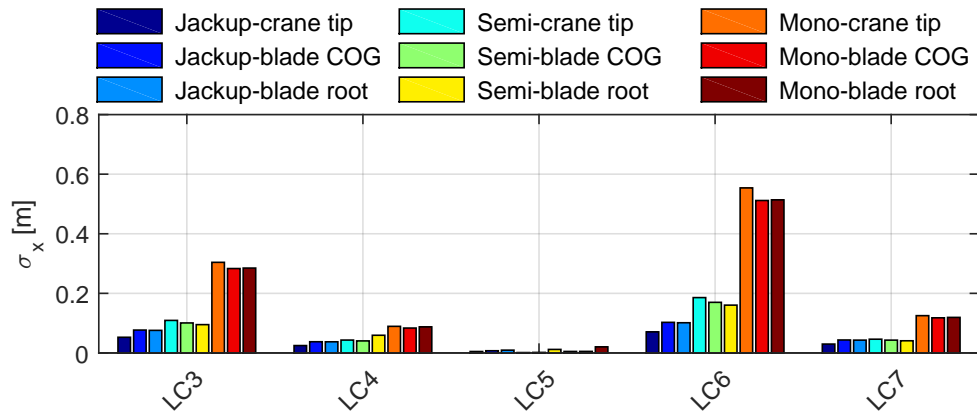
6.2.6. Comparison of motions in the global coordinate system

The translational movements at crane tip, blade COG and blade root are further compared in the global coordinate system. Figure 19 shows their corresponding standard deviations.

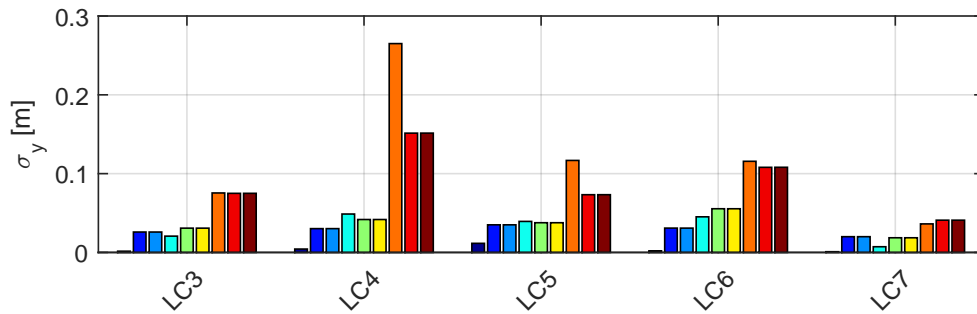
It can be found in Figure 19 that the blade COG movement is quite different from that of the crane tip. When the jack-up crane vessel is used, the former is overall larger than the latter. Nevertheless, the former is observed to be smaller than the latter on the mono-hull vessel, especially along global X and Y directions. Compared to the jack-up and mono-hull vessels, the semi-submersible vessel experiences smaller differences in crane tip and blade COG movement. Besides, the blade root movement along the global Z direction is found to be much larger than that of the blade COG during installations by all three vessels in Figure 19(c). Hence, detailed system modeling is recommended for offshore wind turbine installation, including the modeling of vessel motion, crane dynamics, lifting arrangement and lifted component.

6.3. Tension in tugger lines

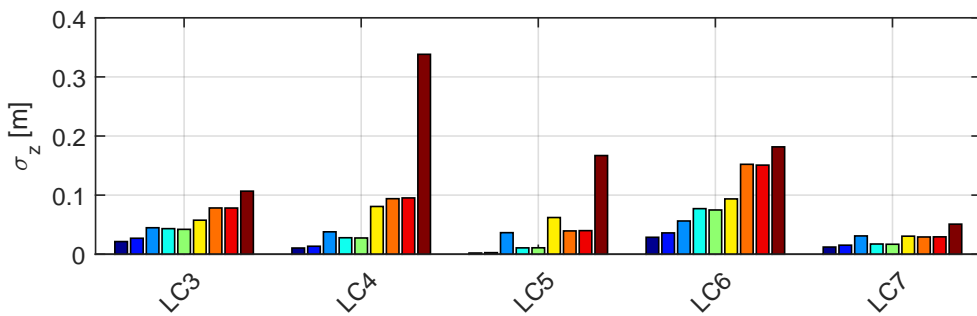
Identical tugger line system with two horizontally deployed tugger lines are used to control the heading of the blade during installation by the three



(a) Along global X axis



(b) Along global Y axis



(c) Along global Z axis

Figure 19: Standard deviation of positions crane tip, blade COG and blade root in the global coordinate system.

crane vessels. The tugger line 1 is close to blade root while tugger line 2 is close to blade tip. During the simulations, no slack event is observed within the tugger lines. The standard deviations of tension in both tugger lines in LC1~LC7 are presented in Figure 20.

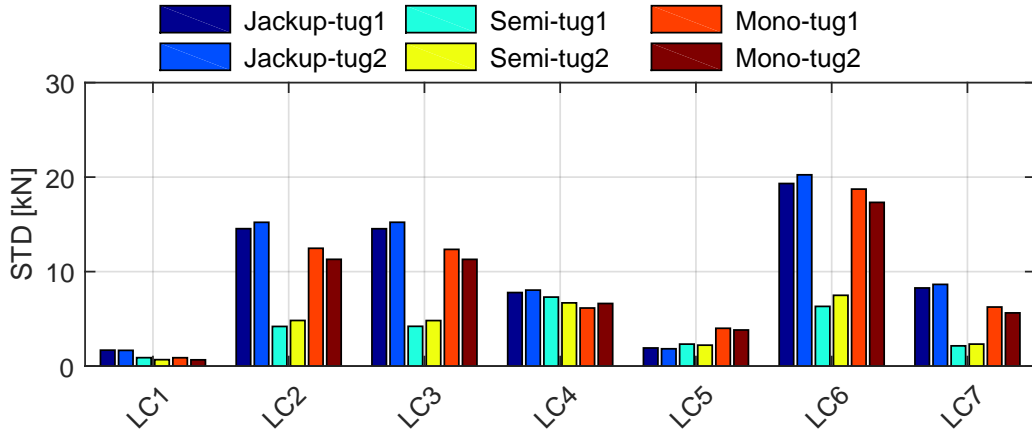


Figure 20: Standard deviations of tension in tugger lines in LC1~LC7

5 The variation of tugger line tension is affected by both wind and wave conditions, as shown by comparing LC1, LC2 and LC3 in Figure 20. However, the latter has highly dominant influence over the former. As a result, the standard deviations of tugger line tension vary significantly with changes in wave conditions, as shown by comparison among LC3~LC7 in Figure 20.

10 The tugger lines on the semi-submersible vessel experience the lowest level of fluctuation in tension. Those on the mono-hull vessel and on the jack-up vessel have a similar level of fluctuation while the former is slightly larger than the latter.

15 Spectral analysis is conducted to further investigate the differences. The results are presented in Figure 21. The tugger line tension for the jack-up

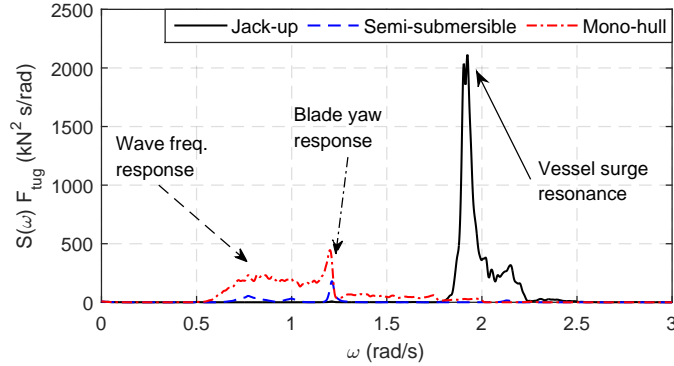


Figure 21: Power spectra of tension in tugger line 1 in LC3

crane vessel is dominated by the vessel surge resonant and crane resonant responses. For the mono-hull vessel, the main contributions are the wave frequency response and the blade yaw resonant response. The tugger line tension for the semi-submersible vessel gets low excitations in all three parts, and thus has the lowest fluctuation.

6.4. Discussion

During single blade installation for offshore wind turbines, the critical event occurs during the mating phase, i.e. mating the blade root into the turbine hub. The operation is not feasible or successful if one of the following scenarios occur during the mating phase:

- Too large blade root displacement in the radial direction of the hub opening, since it can make mating operation not possible.
- Excessive blade root velocity, especially in the radial direction of the hub opening, since it can cause impact with the hub opening and consequently damage guide pins at the blade root. It should be noted that

the guide pins are much stronger in taking axial force than bending moment (Verma et al., 2018).

Therefore, the blade root displacement and velocity in the radial direction of the hub opening are two critical parameters that strongly affect the feasibility of single blade installation. Nevertheless, relevant quantitative criteria with respect to these two critical parameters are difficult to obtain.

In order to assess the feasibility of single blade installation offshore by floating crane vessels in the present study, the criteria are taken as the characteristic values of blade root displacement and velocity in the radial direction of the hub opening during installation by a typical jack-up crane vessel. Figure 15 indicates that among the LCs considered, LC6 gives the largest blade root displacement during installation by the jack-up crane vessel. Hence the characteristic blade root displacement and velocity in LC6 installed by the jack-up crane vessel are assumed to be the criteria. It should be noted that the criteria considered are conservative as the environmental conditions in LC6 are below the operational limits for installation by jack-up crane vessels.

Figure 22 presents the comparison of blade root displacement and velocity in the radial direction of the hub opening in LC8, against the selected criteria. The wave peak period T_p varies in LC8 while the significant wave height ($H_s = 1m$) and wind condition are kept constant. As shown in Figure 22, both R_{xz} and V_{xz} increase significantly with increasing T_p . Single blade installation by the mono-hull crane vessel is feasible under wave conditions with T_p less than 7s. The semi-submersible vessel installation is feasible with a larger T_p of about 8s. Therefore, the feasibility of single blade installation by floating vessels is dependent on the probability of peak period T_p , or the

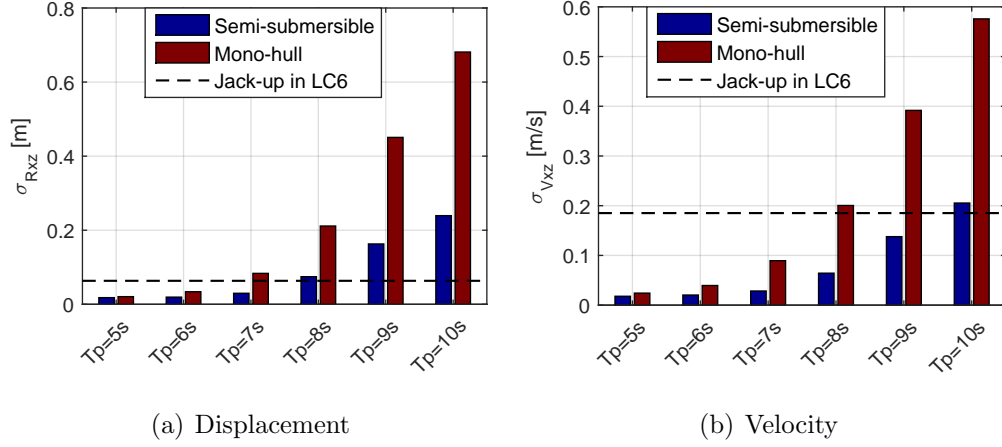


Figure 22: Comparison of blade root motion (displacement and velocity) in the radial direction of the hub opening in the global coordinate system during installation by floating vessels in LC8 (with varying wave peak period) to the corresponding values of the jack-up crane vessel in LC6.

probability of operational weather window.

The feasibility of single blade installation by floating vessels is expected to be larger at offshore wind farm sites characterized by relatively short waves, such as in the North Sea, rather than sites dominated by long waves. Because
 5 the blade during installation by floating vessels has smaller motion in short waves than in long waves, as shown in Figure 22.

The semi-submersible vessel has a larger feasibility with respect to single blade installation, compared to the mono-hull vessel. Because the blade motion is larger when installed by the mono-hull vessel, due to larger wave-
 10 induced vessel motion partially caused by the difference in vessel displacement. The displacement of the mono-hull vessel considered is about 40% of the semi-submersible vessel. The mono-hull vessel's performance is expected to be improved by increasing the vessel size. However, the geometrical layout

of the mono-hull vessel results in motion natural periods close to (or within) typical wave period range, e.g., in heave, roll and pitch.

To increase feasibility and performance of floating crane vessels in single blade installation, the vessels should be carefully selected. Increase of vessel size is one possible solution from the technical point of view, but it will
5 increase the vessel construction cost and consequently the operational cost. Another possible solution is to use a floating vessel with better hydrodynamic performance, e.g., with natural periods of vessel motion outside typical wave period range. A suitable vessel type is semi-submersible. The geometrical
10 parameters of a semi-submersible vessel, such as pontoons, columns, cross section and overall size, usually can make its natural periods of motion beyond upper limit of typical wave periods.

Utilization of weather orientation is another way to improve the floating vessels' performance when installing wind turbine blades, as shown by comparing LC3~LC5 in Figure 23. By adjusting the vessel heading relative to
15 the wave direction, such as head sea in LC5, the blade root radial motion is greatly reduced for both of the floating vessels.

Floating crane vessels can more easily be relocated during offshore wind turbine installation, than jack-up vessels. The installation process of a jack-up vessel, such as leg lowering and retrieval, is sensitive to wave conditions
20 and very time consuming (over 4 hours in total) (Fred. Olsen Windcarrier AS, 2016). Nevertheless, it is not necessary for floating vessels, and hence the time spent on relocation can be significantly shorter.

It should be noted that this paper focuses on a preliminary feasibility
25 study of offshore single blade installation by floating crane vessels, therefore,

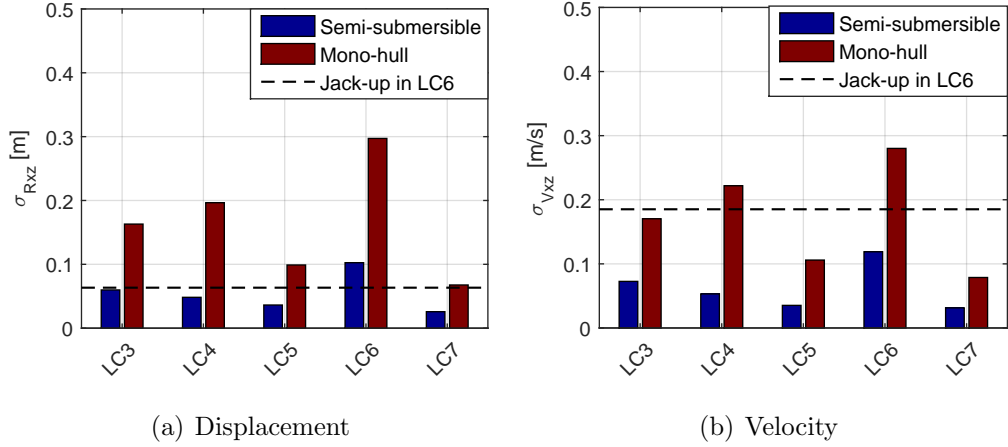


Figure 23: Comparison of blade root motion (displacement and velocity) in the radial direction of the hub opening in the global coordinate system during installation by floating vessels in LC3~LC7 (correlated wind and wave conditions) to the corresponding values of the jack-up crane vessel in LC6.

only a limited number of wind and wave conditions are considered. The wind and wave conditions in LC3~LC7 are correlated and they are based on the long term hindcast data from the North Sea Center Site (Li et al., 2015).

The feasibility of floating vessel installation in this study is evaluated from the perspective of vessel performance. However, there are also many other factors to be considered when selecting vessels during planning phase of operations, such as environmental conditions, vessel availability, budget of operation, etc., which need specific coordination according to projects.

7. Conclusions

This paper deals with a feasibility study of using floating crane vessels during installation of offshore wind turbine blades, by a detailed comparison of system dynamic responses with a typical jack-up crane vessel. The com-

parison is conservative because the installation of a jack-up vessel is weather sensitive. Two typical floating crane vessels, i.e., a mono-hull vessel and a semi-submersible vessel, are considered to install the DTU 10 MW wind turbine blade. The floating vessels are assumed to be equipped with good
5 dynamic positioning systems to mitigate the slowly varying horizontal motions. Fully coupled time domain simulations are carried out to investigate the dynamic responses of the three blade installation systems, including the motions of the vessel, the crane tip, the installed blade and the blade root, and tension in tugger lines.

10 The crane tip movement caused by the crane's elastic deformation plays a relatively less important role in blade installation by floating crane vessels, than for the jack-up crane vessel. This is because the crane tip motion on the floating vessels mainly follows the vessels' rigid body motion. The semi-submersible vessel causes much smaller blade motion than the mono-hull
15 vessel. It also causes much smaller variation of the tugger line tension than the mono-hull vessel and the jack-up vessel.

It is feasible to use floating crane vessels to install offshore wind turbine blades provided that the slowly varying motion of floating vessels are well mitigated by the DP system. The feasibility lies in the allowable operational
20 weather window, and is site- and vessel-dependent. Offshore sites with short wave conditions has higher feasibility in floating vessel installation than at sites with long wave conditions. Floating vessels with small wave frequency motion responses are expected to have a higher feasibility. Utilization of weather orientation for floating vessels can greatly reduce the motion of the
25 installed blade and hence increase the feasibility and reduce the operational

cost.

Acknowledgment

The authors appreciate the support from the Department of Marine Technology, Centre for Ships and Ocean Structures (CeSOS) and Centre for Autonomous Marine Operations and Systems (AMOS), NTNU. Thanks are extended to Mr. Petter Faye Søyland and Mr. Eric Van Buren in Fred Olsen Windcarrier for valuable input data of and discussions on the numerical modeling of the jack-up crane vessel. Thanks are also extended to Dr. Chenyu Luan for valuable discussions.

10 Reference

- Acero, W. G., Gao, Z., Moan, T., 2017. Methodology for assessment of the allowable sea states during installation of an offshore wind turbine transition piece structure onto a monopile foundation. *Journal of Offshore Mechanics and Arctic Engineering* 139 (6), 061901.
- 15 Ahn, D., Shin, S.-C., Kim, S.-Y., Kharoufi, H., Kim, H.-C., 2017. Comparative evaluation of different offshore wind turbine installation vessels for Korean west-south wind farm. *International Journal of Naval Architecture and Ocean Engineering* 9 (1), 45–54.
- Bak, C., Zahle, F., Bitsche, R., Kim, T., Yde, A., Henriksen, L. C., Hansen, 20 M. H., Natarajan, A., 2013. Description of the DTU 10 MW reference wind turbine. Tech. Rep. DTU Wind Energy Report-I-0092, Technical University of Denmark.

- DNV, 2007. DNV-RP-C205 Environmental conditions and environmental loads. Standard, DET NORSKE VERITAS, Oslo, Norway.
- DNV, 2014. Recommended Practice DNV-RP-H103, Modelling and Analysis of Marine Operations. Standard, DET NORSKE VERITAS, Oslo, Norway.
- 5 Fred. Olsen Windcarrier AS, 2016. Specifications for Jack-up Installation vessels Brave Tern and Bold Tern. Report, Fred. Olsen Windcarrier AS, Oslo.
- Hoerner, S. F., Borst, H. V., 1985. Fluid-dynamic lift: practical information on aerodynamic and hydrodynamic lift. Hoerner Fluid Dynamics, Vancouver,
10 ver, WA.
- Horner, S., 1965. Fluid dynamic drag: Practical information on aerodynamic drag and hydrodynamic resistance. Hoerner Fluid Dyn., Midland Park, NJ.
- Jiang, Z., Gao, Z., Ren, Z., Li, Y., Duan, L., 2018. A parametric study on
15 the final blade installation process for monopile wind turbines under rough environmental conditions. Engineering Structures 172, 1042–1056.
- Jonkman, B. J., 2009. Turbsim user’s guide: Version 1.50.
- Keseric, N., 2014. Norway’s solution: Hywind world’s first full scale floating turbine. Report, Statoil.
- 20 Ku, N., Roh, M.-I., 2015. Dynamic response simulation of an offshore wind turbine suspended by a floating crane. Ships and Offshore Structures 10 (6), 621–634.

- Li, L., Gao, Z., Moan, T., 2015. Joint distribution of environmental condition at five european offshore sites for design of combined wind and wave energy devices. *Journal of Offshore Mechanics and Ocean engineering* 137 (3), 031901.
- 5 Paterson, J., D'Amico, F., Thies, P., Kurt, R., Harrison, G., 2018. Offshore wind installation vessels—A comparative assessment for UK offshore rounds 1 and 2. *Ocean Engineering* 148, 637 – 649.
- Pedersen, E. A., 2012. Motion analysis of semi-submersible. Master's thesis, Department of Marine Technology, Norwegian University of Science and
10 Technology.
- Sarkar, A., Gudmestad, O. T., 2013. Study on a new method for installing a monopile and a fully integrated offshore wind turbine structure. *Marine Structures* 33, 160–187.
- Seaway Heavy Lifting, 2018. Oleg strashnov. <https://www.seawayheavylifting.com.cy/vessels/oleg-strashnov>,
15 (Accessed on 04/15/2018).
- Shi, W., Park, H.-c., Chung, C.-w., Kim, Y.-c., et al., 2011. Comparison of dynamic response of monopile, tripod and jacket foundation system for a 5-mw wind turbine. In: *The Twenty-first International Offshore and Polar
20 Engineering Conference*, Hawaii, USA, June 19-24, 2011.
- SINTEF Ocean, 2017a. RIFLEX- Theory Manual 4.10.1. SINTEF Ocean, Trondheim, Norway.

SINTEF Ocean, 2017b. SIMO-Theory Manual Version 4.10. SINTEF Ocean, Trondheim, Norway.

SINTEF Ocean, 2017c. SIMO-User Manual Version 4.10. SINTEF Ocean, Trondheim, Norway.

5 Statoil, 2018. Hywind-the leading solution for floating offshore wind power. <https://www.statoil.com/en/what-we-do/hywind-where-the-wind-takes-us.html>, (Accessed on 05/01/2018).

Verma, A. S., Jiang, Z., Vedvik, N. P., Gao, Z., Ren, Z., 2018. Impact assessment of a wind turbine blade root during an offshore mating process.
10 Engineering structures (under review).

Wind Europe, 2018. Offshore wind in Europe- Key trends and statistics 2017. Report, Wind Europe.

Zhao, Y., Cheng, Z., Sandvik, P. C., Gao, Z., Moan, T., 2018a. An integrated dynamic analysis method for simulating installation of a single blade for
15 offshore wind turbines. Ocean Engineering 152, 72–88.

Zhao, Y., Cheng, Z., Sandvik, P. C., Gao, Z., Moan, T., Buren, E. V., 2018b. Numerical modeling and analysis of the dynamic motion response of an offshore wind turbine blade during installation by a jack-up crane vessel. Ocean Engineering (under review).

20 Zhu, H., Li, L., Ong, M., 2017. Study of lifting operation of a tripod foundation for offshore wind turbine. In: IOP Conference Series: Materials Science and Engineering. Vol. 276(1). p. 012012.